Mon. Not. R. Astron. Soc. **000**, 1–**??** (2015) Printed 2 June 2015 (MN LATEX style file v2.2)

Multi-band variability in the blazar 3C 273 with XMM-Newton

Nibedita Kalita[1,2], Alok C. Gupta[1⋆], Paul J. Wiita[3], Jai Bhagwan[1,4], Kalpana Duorah[2]

[1]*Aryabhatta Research Institute of Observational Sciences (ARIES), Manora Peak, Nainital, 263 002, India*
[2]*Department of Physics, Gauhati University , Guwahati,781 014,India*
[3]*Department of Physics, The College of New Jersey, P.O. Box 7718, Ewing, NJ 08628-0718, USA*
[4]*School of Studies in Physics & Astrophysics, Pt Ravishankar Shukla University, Amanaka G.E. Road, Raipur 492010, India*

ABSTRACT

We have undertaken a nearly simultaneous optical/UV and X-ray variability study of the flat spectrum radio quasar, 3C 273 using data available from the XMM−Newton satellite mission from June 2000 to July 2012. Here we focus on the multi-wavelength flux variability on both intra-day and long time scales of this very well known radio-loud source. We found high flux variability over long time scales in all bands for which observations were made. The optical/UV variability amplitude was more than twice than that in the X-ray bands. There is some frequency dependence of the variability in optical/UV bands in the sense that the variability amplitude increases with increasing frequency; however, the X-ray emissions disagree with this trend as the variability amplitude decreases from soft to hard X-ray bands. On intra-day time scales 3C 273 showed small amplitude variability in X-ray bands. A hardness ratio analysis in the X-ray regime indicates that the particle acceleration mechanism dominates the cooling mechanism during most of the ∼12 year span of these observations.

Key words: galaxies: active – quasars: general – quasars: individual: 3C 273 – X-rays: individual: 3C 273

1 INTRODUCTION

The subclasses of radio-loud active galactic nuclei (AGN) that include BL Lac objects (BLLs) and flat spectrum radio quasars (FSRQs) are collectively known as blazars. The optical spectra of BLLs show featureless continua whereas spectra of FSRQs have prominent emission lines. Blazars show rapid flux variability across the complete electromagnetic (EM) spectrum, have high and variable polarization and their emission is predominantly non-thermal. Their radio structures are dominated by compact cores. Blazars also show superluminal motion due to Doppler boosting and thus are understood to possess relativistic jets of highly collimated radiation and plasma emanating from the central region viewed at a small ($\lesssim 10^{\circ}$) angle to the line of sight of the observer (Urry & Padovani 1995). In the case of FSRQs the accretion disc component (big blue bump) can be seen in their multi- wavelength spectral energy distributions (SEDs) on occasions when the FSRQs are observed in their low flux state, whereas BLLs show weak or absent emission from the disc.

Blazars show flux variations in all bands of the EM spectrum on all possible timescales. Those fluctuations ranging from a few tens of minutes (and sometimes even more rapid) to less than a day in our observer's frame are often known as intra-day variability (IDV) (Wagner & Witzel 1995). Variability with time scales of few days to weeks is commonly known as short term variability (STV), while variability on time scales ranging from months to the longest we have monitored (typically several years) is called long term variability (LTV) (e.g., Gupta et al. 2004). The IDV in blazars is the least well understood type of variations but it can provide an important tool for learning about structures on small spatial scales and it also provides us with better understanding of the different radiation mechanisms that are important in the emitting regions (e.g., Wagner & Witzel 1995). Any characteristic time scale of variability can effectively provide us with information about the physical structure of the central region and complex phenomena such as hot spots on accretion discs (e.g., Mangalam & Wiita 1993). In blazars, it is widely believed that most variability originates mainly from enhanced emission in a small region within the relativistic jets (e.g., Begelman et al. 2008). For example, excess emission could be triggered by dissipation inside a blob of material emerging from at the jet base, from shocks propagating along the jet, or from instabilities within the jet itself.

3C 273 ($\alpha_{2000.0} = 12\mathrm{h}29\mathrm{m}06.7\mathrm{s}$, $\delta_{2000.0} = +02^{\circ}03^{'}09^{"}$, z =0.158339) was the first quasar discovered in the radio sky survey at 158 MHz that was included in the third Cambridge (3C) catalogue (Edge et al. 1959). In early 1963, it was classified as a FSRQ (Schmidt 1963). Unsurprisingly, this relatively nearby blazar has been extensively studied on diverse time scales across the com-

⋆ Email: acgupta30@gmail.com

plete EM spectrum, with measurements made in single bands and often as well as in multi-bands (Mantovani et al. 2000; Collmar et al. 2000; Sambruna et al. 2001; Greve et al. 2002; Kataoka et al. 2002; Courvoisier et al. 2003; Jester et al. 2005; Attridge et al. 2005; Savolainen et al. 2006; McHardy et al. 2007; Soldi et al. 2008; Pacciani et al. 2009; Dai et al. 2009; Fan et al. 2009, 2014; Abdo et al. 2010; and references therein).

This source has been studied in optical bands since its discovery. Optical (V, R and I band) studies show the variable flux in the source changes with different amplitudes on different timescales revealing the nonlinear variability characteristic of blazars. It was also noticed that, at higher frequencies, the strength of the flux variations in 3C 273 are higher than in the lower frequencies (e.g., Fan et al. 2009). This type of frequency dependent variability is also valid for near-infrared bands (Wen et al. 2002). While monitoring the source in optical bands from 1998 to 2008, Fan et al. (2014) found that during this period the source did not show very significant IDV but it showed strong LTV. Imaging data from *Hubble Space Telescope* in the UV show compatibility of far-UV with extrapolated 0.5-8 keV X-ray flux, thereby supporting a common origin of UV and X-ray emissions in the relativistic jet (Jester et al. 2007). Long-term optical observations in BVRI bands from 2003 to 2005 with the Yunnan National Astronomical Observatory (YNAO) 103 cm telescope and Shanghai Astronomical Observatory (SHAO) 156 cm telescope show that the source was in a rather steady flux state during this campaign (Dai et al. 2009). The same study shows strong inter-band correlations of color index and magnitude in the optical regime, where the spectrum becomes flatter when the source brightens and softer when the source brightness decreases for both IDV and LTV, which is similar to spectral evolution of most BL Lacs.

Soldi et al. (2008) used various ground and space based telescope data to study the variability in the source over almost the entire EM spectrum (i.e., radio to $\gamma-$rays) for about a decade. Their study revealed energy dependent variability time scales and variability amplitudes of 3C 273. The variability in X-ray bands indicate the presence of two different components, one of them which can be considered Seyfert-like while the other is blazar-like. A contemporary study of the source with BeppoSAX and XMM-Newton interprets the Seyfert-like component and soft excess as the result of a non-thermal flare-like coronal model (Pietrini et al. 2008). The hard X-ray variability correlated with long term optical variability but not to radio variability, which indicates that the emission mechanism for hard X-rays ($\geqslant$ 20 keV) is not due to electrons accelerated by the shock waves in the jet but probably arises from inverse Compton scattering of synchrotron optical photons emitted from a region near the base of the jet by the same electron population (Soldi et al. 2008).

A soft X-ray study of 3C 273 by ROSAT showed short term variability of about 20 per cent over $\sim$ 2 days (Leach et al. 1995). RXTE observations of the source at hard X-ray bands found similarly modest variations over several days but variability up to a factor of four over four years (Kataoka et al. 2002). The high correlation between X-ray ($3-20$ keV) and IR fluxes provides evidence for the origin of X-ray emission in 3C 273 being a result of the Compton scattering of low-energy seed photons (McHardy et al. 1999). However, the X-ray emission from 3C 273 shows different timing properties for variability below and above $\sim$ 20 keV and this produces uncertainty about the origin of the hard X-ray emission, which was previously considered to be part of the jet emission (Soldi et al. 2008).They have studied fractional variability amplitude and characteristic time scale with structure function (SF) analysis using XMM-Newton data from 2000–2005. This analysis technique to study variability has been used frequently by the community. Turriziani (2011) & Vagnetti et al. (2011) seperately performed SF to study the X-ray variability for this source with XMM-Newton data. The later work (Vagnetti et al. (2011)) found that the variability is anti-correlated with X-ray luminosity. During the period 2000–2009, Liu & Zhang (2011) studied STV in soft and hard X-ray bands with the help of XMM-Newton satellite, and they reported that soft and hard X-rays come from different origins. Brightman & Nandra (2012) used classical hardness ratio to find an effective colour–colour selection for obscured AGN from X-ray data using a sample of heavily absorbed active galactic nuclei (including 3C 273).

A recent study has indicated that the physical process initiating variability in the X-ray domain of 3C 273 is similar to that in Seyfert galaxies (McHardy 2013). 3C 273 has long been known to have a soft excess in the X-ray band at $\leqslant$ 1 keV (Turner et al. 1985). Many studies have shown a soft excess at energies ranging from 0.1 keV $-$ 2 keV (Courvoisier et al. 1987; Page et al. 2004; Türler et al. 2006; Chernyakova et al. 2007; Pietrini et al. 2008; and references therein). It was also detected as one of the first extragalactic $\gamma-$ray sources by the COS-B satellite (Swanenburg et al. 1978).

A wavelet analysis of X-ray time series data of 3C 273 taken by XMM–Newton indicated a candidate 3.3 ks quasi-periodic oscillation (QPO; Espaillat et al. 2008). With the assumption that the QPO is generated near the last stable orbit in the accretion disk the central black hole mass is constrained to lie between $7.3 \times 10^6\ M_\odot$ if it is a Schwarzschild BH and $8.1 \times 10^7\ M_\odot$ for a maximally rotating Kerr black hole. However, previous reverberation-mapping estimates gave much higher masses of $2.35 \times 10^8 M_\odot$ (Kaspi et al. 2000) and $6.59 \times 10^9 M_\odot$ (Paltani & Türler 2005) which would imply that this QPO is not due to the dynamical motion in the inner accretion disk, but perhaps due to oscillation modes in the accretion disc (Espaillat et al. 2008). Subsequent studies have, however, called into question the presence of a QPO in 3C 273 (Mohan et al. 2011; González-Martín & Vaughan 2012).

Although the emission mechanism for blazars is not yet completely understood, it is clear that the lower energy photons arise from synchrotron emission and in many cases this emission extends into the soft part of the X-ray band. Contributions from synchrotron self-Compton (SSC) and external Compton (EC) are the two main candidate mechanisms to dominate the harder part of X-ray emission and produce the γ-ray emission. The harder X-ray emission also can have a contribution from the Compton scattering of disc photons by the hot corona sandwiching the disc (Sikora 1994, Ghisellini & Tavecchio 2008). Studies have also shown strong correlation between IR and X-ray emission from time to time, in the sense that the IR leads the X-ray emission, supporting the SSC model (McHardy et al. 2007).

Multi-wavelength (optical, UV and X-ray) LTV and interband correlation of this source with XMM-Newton data available till date (2012) is done for the first time by us in the present work. LTV of 3C 273 in X-ray bands was studied previously in different time period by differet groups, but here we study LTV of this source for the longest period ever done in X-ray bands, both soft and hard bands using XMM-Newton data. We also study the LTV in optical and UV bands in the same period with Optical Monitor (OM) data, which has not done before. IDV studies on a few occasions are done in past but we have studied here IDV in X-rays with all the time series data available for the source till 2012.

In this paper, we study IDV and LTV of the FSRQ 3C 273. In the next section, we discuss XMM$-$Newton archival data. In sec-

tion 3, the techniques we used for data reduction and light curve generation are given. In section 4, we report our results and in section 5, we present a discussion and the conclusions of the work.

2 XMM−NEWTON ARCHIVAL DATA

2.1 X-ray Data

3C 273 has been frequently observed with different telescopes over different frequency ranges. The European X-ray satellite mission, XMM−Newton is one of the rare instruments that is capable of observing a particular source in multiple bands simultaneously, in this case in the Optical, UV and X-ray bands. The X-ray collecting area of the telescope is huge and targets can be exposed for very long periods without any interruption, allowing this satellite to produce sensitive observations in the energy range from 0.15 to 15 keV. The EPIC cameras provide imaging observations taken with a very large (30 arcmin) field of view (FOV). These specifications make this satellite perfect for our purpose of studying the relation between different bands and their emitting regions. XMM−Newton has observed 3C 273 for over a decade in time in X-ray, optical and UV making it possible for us to study variability on different time scales.

In this paper we have used XMM−Newton satellite data to study the behaviour of the source in all three bands. Observation data files (ODFs) were downloaded from the on-line XMM-Newton science archive. For reduction of these data we have used XMM-Newton Science Analysis Software (SAS) version 12.0.1. The on board system of XMM−Newton contains the European Photon Imaging Camera (EPIC), which consists of two CCD arrays, MOS and pn. Here we have used EPIC/pn camera observations for our purpose, since the sensitivity of EPIC/pn is much higher than that of the MOS camera (e.g. Strüder et al. 2001). XMM–Newton has data for the source 3C 273 from June 13, 2000 to July 16, 2012 which is comprised of a total of 34 observations in XMM–Newton science archive. However, out of these 34 observations two observation IDs do not contain any data, and pn data was not available for four other observation IDs. Three more observations were excluded because of their bad image quality. So here we have studied 25 observations for the source 3C 273.

2.2 Optical/UV Data

The Optical/UV Monitor Telescope (OM hereafter) on board XMM–Newton provides the facility to observe simultaneously a particular source in optical and UV bands along with the X-ray bands, with a very high imaging sensitivity (e.g. Mason et al. 2001). This makes possible the study of the relationship between the emission mechanisms corresponding to these bands. The OM can collect data with time resolution of 0.5 s for the wavelength range 170 nm – 650 nm with six broad band filters, three in the optical and three in the UV, with a FOV covering 17 arcmin of the central region of the X-ray telescope FOV. The optical *U, B, V*, filters collect data in the wavelength ranges 300–390 nm, 390–490 nm, 510–580 nm, respectively and the ultraviolet *UVW2, UVM2, UVW1* filters collect data in the wavelength ranges 180–225 nm, 205–245 nm, and 245–320 nm, respectively. 3C 273 was observed with OM for differing numbers of exposures for different observing periods (see Table 1 for details). The source was simultaneously observed with both X-ray and Optical/UV telescopes for a total of 16 observation IDs.

3 DATA ANALYSIS TECHNIQUES

3.1 Light Curve generation

The EPIC/pn camera takes images of a target source for the energy range 0.15−15 keV, but data above 10 keV are dominated by strong proton flaring. X-rays emitted below 0.3 keV are highly affected by hydrogen in the direction of 3C 273 in our own galaxy. Moreover, the on-axis effective area of the EPIC pn camera play an important role in the performance of the X-ray mirrors. These mirrors can reflect X-ray photons most efficiently in the energy range from 0.1 to 10 keV. Therefore, for better quality and higher accuracy of the data set, we choose the energy range from 0.3−10 keV for the light curve extraction. By doing this we automatically eliminate the effect of absorption in the lower energy range and the background noise in the higher energy range. All EPIC/pn observations we have used were taken in small window (SW) mode.

Event files of the pn detector were generated through *epchain*. Before generating a cleaned event list, first we generated a light curve for energy range of 10–12 keV and saw the soft proton flares effect on this and then generated a good time interval file using the *TABGTIGEN* tool which contains information of the good times that are free from soft proton flares. In the next step, we used the event list file and GTI files as input to obtain cleaned event files and we later filtered the data using the condition $(PATTERN \leqslant 4)$ energy range 0.3−10 keV and $(FLAG{=}0)$. With cleaned event files, we have generated source images and for source event files, the bright circular source region of 40 arcsec radius is selected in such a way that 90 per cent of the source flux lies inside the circle, for background event files, we selected a circular region of maximum possible size (which ranged between 40−50 arcsec for different images/CCD chips), but as far away as possible on the same CCD chip to avoid any contribution from the source region.

Pile up is a common problem for very bright sources like our blazar and was an issue for seven observation IDs. Pile up occurs when two or more X-ray photons fall on a single CCD pixel before the instrument's read out time, and as a result, the CCD will recognize these separate photons as a single one with energy equal to the sum of the individual energies of the two or more photons. It also may arise when more than one photon is detected by two or more adjacent pixels during a single read-out cycle. This pile up problem is detected by using *epatplot* routine for all the observation IDs and later they were removed by selecting an central annulus region instead of circular region for both the source events file and background events file as used before in non-pile up affected observations on the same CCD chip. Since all observations we have used here in our study were carried out in small window mode (time resolution = 5.7 ms), we used a binning of 114 seconds, which is an integer multiple of the instrument time resolution. We obtain the final corrected events list by subtracting the background counts from the source counts. The events list files obtained by using the *epiclccorr* task contains some null points occurring when the window of the CCD chip was being closed during that exposure time. Also there are some fictitious points which show significantly larger error bars than the others with a peculiar deviation in counts from the normal order at the start or end in the events list; these originateswhen the source exposure time is less than 70 per cent of the window flag time. These points were removed to generate the final corrected lists. After correcting all these issues, we finally plot the light curves for observations. The 3C 273 public data over the 12 year span is given in Table 1.

We take the imaging mode data of OM for our purpose, which we later reprocessed with the perl script *omichain*, which starts dif-

Table 1. Summary of XMM-Newton data for 3C 273

Date of Obs. dd.mm.yyyy	Obs.ID	Revolution	Window Mode	GTI (ks)	Pile up	Filter	μ (counts s^{-1})	OM filter[1]	Exposures[2]
13.06.2000	0126700101	94	Full Frame	Nil	Nil	MEDIUM	Nil	6	5
13.06.2000	0126700201	94	Full Frame	Nil	Nil	MEDIUM	Nil	6	5
13.06.2000	0126700301	94	Small	64.9	No	MEDIUM	47.04±0.81	1,2,3,4,5,6	29
15.06.2000	0126700401	95	Full Frame	Nil	Nil	MEDIUM	Nil	6	5
16.06.2000	0126700501	95	Full Frame	Nil	Nil	MEDIUM	Nil	6	5
15.06.2000	0126700601	95	Small	29.6	No	MEDIUM	45.41±0.80	4,5,6	15
15.06.2000	0126700701	95	Small	29.9	No	MEDIUM	44.16±0.80	1,2,3	15
17.06.2000	0126700801	96	Small	60.1	No	MEDIUM	44.26±0.79	1,2,3,4,5,6	30
13.06.2001	0136550101	277	Small	88.5	Yes	MEDIUM	21.58±0.58	1,2,3,4,5,6	12
16.12.2001	0112770101	370	Small	4.9	No	THIN1	71.95±1.00	Nil	Nil
22.12.2001	0112770201	373	Small	4.9	No	THIN1	69.50±0.99	Nil	Nil
09.01.2002	0137551001	382	Burst	Nil	Nil	MEDIUM	Nil	6	1
07.07.2002	0112770601	472	Small	4.9	No	THIN1	53.93±0.87	Nil	Nil
17.12.2002	0112770801	554	Small	4.9	No	THIN1	77.54±1.04	Nil	Nil
05.01.2003	0112770701	563	Small	4.9	No	THIN1	65.32±0.96	Nil	Nil
05.01.2003	0136550501	563	Small	8.4	No	MEDIUM	63.22±0.94	2,3	2
18.06.2003	0112771001	645	Small	5.4	No	THIN1	80.24±1.09	Nil	Nil
07.07.2003	0159960101	655	Small	58.0	Yes	THIN1	26.05±0.57	1,3,4,5,6	5
08.07.2003	0112770501	655	Small	8.0	No	THIN1	70.66±1.04	Nil	Nil
14.12.2003	0112771101	735	Small	8.3	No	THIN1	53.34±0.87	Nil	Nil
30.06.2004	0136550801	835	Small	19.7	No	MEDIUM	45.27±0.81	1,2,3,4,5,6	6
10.07.2005	0136551001	1023	Small	27.5	No	MEDIUM	49.68±0.84	1,2,3,4,5,6	6
12.01.2007	0414190101	1299	Small	76.5	Yes	MEDIUM	21.42±0.52	1,2,3,4,5,6	9
25.06.2007	0414190301	1381	Small	31.9	No	MEDIUM	45.90±0.80	1,2,3,4,5,6	8
08.12.2007	0414190401	1465	Small	35.3	Yes	MEDIUM	38.16±0.69	1,2,3,4,5,6	6
09.12.2008	0414190501	1649	Small	40.4	Yes	THIN1	21.57±0.52	1,2,3,4,5,6	6
20.12.2009	0414190601	1837	Small	31.3	Yes	THIN1	24.36±0.57	Nil	Nil
10.12.2010	0414190701	2015	Small	35.8	Yes	THIN1	18.29±0.48	1,2,3,4,5,6	6
12.12.2011	0414190801	2199	Small	42.8	No	THIN1	47.48±0.82	1,2,3,4,5,6	6
16.07.2012	0414191001	2308	Small	25.5	No	THIN1	41.22±0.93	4,5,6	3

μ = mean count rate;
GTI = Good Time Interval
[1] 1 = *UVW2*, 2 = *UVM2*, 3 = *UVW1*, 4 = *U*, 5 =*B*, 6 = *V*
[2] Total number of exposures combining all six filters

ferent tasks within SAS for full processing of OM data. After running the metatask *omichain*, we get a observation source list which contains the calibrated data with their errors. The source list contains several objects and their corresponding data points are treated as background points. The objects near to the source co-ordinate appear in the source FOV with similar RA and DEC values. We identify our source from this object list by selecting the right RA and DEC value for our source.

Since the blazar is among the brightest objects in the OM FOV, the source will have very large counts rate in all filters.

3.2 Excess Variance

Blazars show very rapid flux variability in all wave bands from radio to $\gamma-$rays. To measure the strength of variability, the commonly used parameters are excess variance, σ^2_{XS} and fractional rms variability amplitude, F_{var}, (e.g. Edelson et al. 2002). Each light curve obtained from different exposures contains information on flux measurements (count rates) with its uncertainties caused by measurement errors for different time intervals. Excess variance gives the intrinsic variance of the source by removing the variance due to measurement errors in each individual flux measurement. When the light curve consist of total number n of flux measurements x_i, at times t_i, with corresponding errors in measurements $\sigma_{err,i}$, then the excess variance is calculated as

$$\sigma^2_{XS} = S^2 - \overline{\sigma^2_{err}}, \tag{1}$$

where $\overline{\sigma^2_{err}}$ is the mean square error and S^2 is the sample variance of the light curve given by

$$S^2 = \frac{1}{n-1}\sum_{i=1}^{n}(x_i - \overline{x})^2 \tag{2}$$

and

$$\overline{\sigma^2_{err}} = \frac{1}{n}\sum_{i=1}^{n}\sigma^2_{err,i}. \tag{3}$$

The fractional rms variability gives the average variability amplitude with respect to the mean flux of a source, which is nothing but the square root of the normalized excess variance, σ^2_{NXS}, which is

$$\sigma^2_{NXS} = \frac{\overline{\sigma^2_{XS}}}{\overline{x}^2} \tag{4}$$

so

$$F_{var} = \sqrt{\frac{S^2 - \overline{\sigma^2_{err}}}{\bar{x}^2}} \tag{5}$$

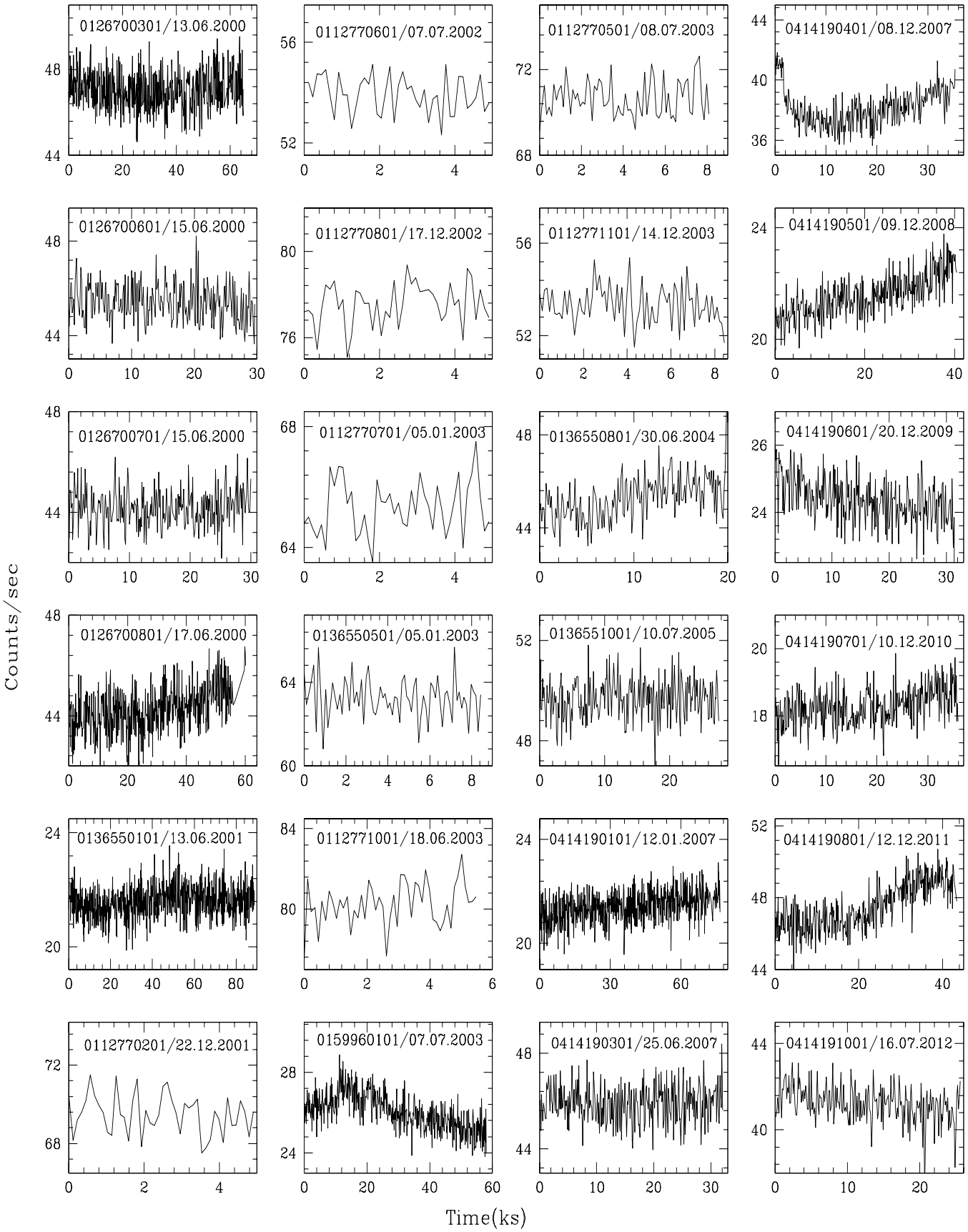

Figure 1. The variation of X-ray photons with time for 3C 273, for observations carried out at different times. The caption on each light curve represents observation ID and observing date, respectively. These light curves were extracted using 114 seconds time binning in the energy range, 0.3−10 keV.

The uncertainty on F_{var} has been calculated using Monte Carlo method for n total events (e.g. Vaughan et al. 2003) and is given by

$$(F_{var})_{err} = \sqrt{\left\{\sqrt{\frac{1}{2n}}\frac{\overline{\sigma_{err}^2}}{\bar{x}^2 F_{var}}\right\}^2 + \left\{\sqrt{\frac{\overline{\sigma_{err}^2}}{n}}\frac{1}{\bar{x}}\right\}^2}. \quad (6)$$

4 RESULTS

4.1 Intraday Variability in X-ray light curves

We have searched for IDV in X-ray light curves for those observations given in Table 1 that provided good data and those 24 light curves are plotted in Fig. 1. In Table 2, we have reported the IDV variability parameters which are calculated using excesses variance. It can be clearly seen that the IDV amplitude in the individual observations are low, usually less than 1 per cent and often consistent with 0, given the errors on F_{var}. The highest variability among all the observations taken during this time span is seen in the observation ID 0159960101 in 2003, and is 2.60 per cent, though the variabilities are essentially as large during two other observations (0414190401 and 0414190501). We note that the longer GTI observations produce higher probabilities of detecting clear variations.

In blazars, it is believed that the X-ray emission is a result of synchrotron radiation from highly energetic electrons moving with relativistic speeds in the jet. It can either be direct synchrotron radiation or results from inverse Compton scattering of lower energy photons off the synchrotron emitting electrons. In case of FSRQs X-ray emissions mainly come from inverse-Compton emission, but here in 3C 273, which is a acceptional case regarding the presence of both Seyfert like and blazar like components in its X-ray spectra, X-rays below 2 keV is due to coronal emission from the accretion disk and above 2 keV is dominated by contribution from jet emission (e.g. Page et al. 2004; Pietrini & Torricelli-Ciamponi 2008; Haardt et al. 1998). Blazars show complex emission behaviour in X-ray flaring states. During these states the object can show both soft and hard lags depending on the time required for cooling and acceleration by radiating electrons. From the smallest variability timescale in X-ray band, the size of the central emitting regions of the blazar can be estimated. If IDV is found during the quiet state of the blazar, when the jet is weak or absent, then it may be attributed as result of changes occurring in the accretion disk, which can constrain the structure of the central engine on linear scales (Gupta et al. 2009). Intra-day X-ray variability may also be due to instabilities on or above the accretion disk, caused by its magnetic field that can also lead to generation of oscillations in the disk.

4.2 Long term variation in Optical/UV & X-ray bands

The source has been observed for more than a decade, which makes it possible for us to study its long term variability behaviour in X-rays as well as in Optical/UV bands. We examine long term behaviour of the source 3C 273 by combining the mean count rates for each observation. The temporal behaviour of the source in between 2000 and 2012, in 2 X-ray and 6 Optical/UV bands are plotted in different panels of Fig. 2. By visual inspection, variability is clearly seen in all of these bands.

We split the X-ray light curve into two light curves with the energy ranges being 0.3–2.0 keV for soft X–rays and 4.0–10 keV for hard X–rays. Previous studies (Page et al. 2004, Pietrini and Torricelli-Ciamponi, 2008, Haardt et al. 1998) have found that the disk emission is the origin of X-ray emission below 2 keV in 3C 273, where disk photons scattered off the hot corona above the disk, while emission above 2 keV comes from inverse-Compton scattering of seed photons by the relativistic jet. So we consider the energy range for soft X–ray band is 0.3–2 keV to be dominated by coronal emission but for the main contribution from the jet, we consider the hard band energy range 4–10 keV, in order to reduce contamination from the X–ray corona. Both the soft and hard X–ray light curves show very similar variability patterns. It seems that there was a small flaring in both the X-ray bands in June 2007 with almost no time lag. A similar kind of flare is seen in December 2007, in all the optical/UV bands when the X-ray fluxes are lower. Though we clearly do not have enough data points to formally calculate any time lag it is not unreasonable to estimate a time delay of the flare in Optical/UV bands with respect to the X-ray bands by visual inspection which give the delay of about six months. However, we cannot claim whether there was a correlation between these two emission peaks or if they originate from two independent emitting regions. We did not find any strong flares. But there are evidences of flares from the source on different occasions. Fan et al. (2014) studied the photometric observation of 3C 273 in optical bands from 1998 to 2008, where they reported detection of two peaks in February 2006 and March 2008 in R band. Beaklini et al. (2014) reported a flare at 7 mm wavelength with Itapetinga Radiotelescope, in Brazil in 2010, which they claim as counterpart of gamma-ray flare detected in September, 2009 by ther Fermi / Large Area Telescope (LAT)with a delay of 170 days. Frequent flares were detected by Fermi/LAT in gamma-ray bands in the period September 2009 to April 2010 (Rani et al. 2013).

Over the long term, 3C 273 showed large RMS variability amplitudes. The RMS variability amplitude for *UVW2, UVM2, UVW1, U, B, V* bands and soft and hard X-ray bands are, in per cent $\sim$ 76, 76, 68, 68, 68, 35, 42, and 36, respectively, with respective perccen-

Table 2. X−ray variability parameters

Obs.IDs	Variance	σ_{XS}^2	F$_{var}$ (%)
0112770101	0.82	0.19	0.61±0.40
0112770201	1.04	0.06	0.34±0.66
0112770501	0.71	0.37	0.86±0.27
0112770601	0.56	0.20	0.83±0.42
0112770701	0.79	0.13	0.54±0.47
0112770801	0.95	0.13	0.47±0.46
0112771001	1.16	0.02	0.19±1.00
0112771101	0.69	0.08	0.51±0.46
0126700301	0.76	0.11	0.69±0.15
0126700601	0.63	0.01	0.16±0.85
0126700701	0.55	0.09	0.67±0.24
0126700801	0.77	0.15	0.88±0.14
0136550101	0.30	0.03	0.80±0.21
0136550501	0.90	0.01	0.12±1.47
0136550801	0.85	0.20	0.99±0.22
0136551001	0.60	0.10	0.65±0.23
0159960101	0.79	0.46	2.60±0.11
0414190101	0.33	0.06	1.15±0.17
0414190301	0.62	0.03	0.36±0.37
0414190401	1.44	0.96	2.57±0.12
0414190501	0.56	0.28	2.47±0.16
0414190601	0.48	0.15	1.61±0.20
0414190701	0.30	0.07	1.48±0.23
0414190801	1.58	0.91	2.01±0.10
0414191001	0.69	0.18	1.02±0.28

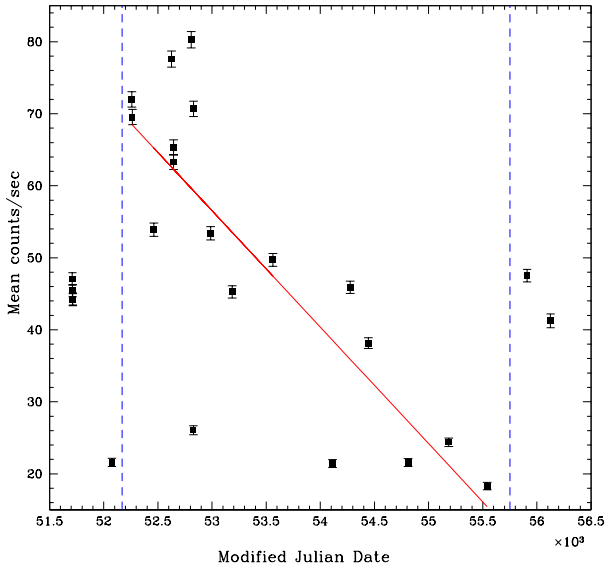

Figure 3. Long term X-ray variability of 3C 273 (2000-2012)

tage errors in variability amplitude of 0.016, 0.0104, 0.0867, 0.76, 0.30, 0.086, 0.475 and 0.983. Thus we conclude that the source is highly variable in both the optical/UV and X-ray domains during the above mentioned time period.

The overall change in the total X-ray flux with time during this observing period of 3C 273 is shown in Fig. 3. On visual inspection, if we exclude small portions of the starting and ending period of this observation there is indication of a linearly decreasing flux profile with time from December 2001 to December 2010. This data is fitted with least squares fitting method and the correlation coefficient for the fit calculated with MATLAB, is -0.8076 and its corresponding null-hypothesis is 0.001. In Fig. 3, the excluded parts of these observations are separated by vertical dotted lines.

4.3 Possible connections between Optical/UV and X-ray bands

From Fig. 2, visually it appears that the optical and UV bands follow the same variability pattern as do the soft and hard X-ray bands. To further examine the variability relations between these optical, UV and X-ray bands, we plotted these bands against each other as shown in Fig. 4. The upper left panel of Fig. 4 explicitly shows that soft and hard X-ray bands are well correlated. In the same manner, to check the correlation in flux variation within broad bands, we plot the optical V band against the B band and in similar way plot the UWV2 band against the UVW1 (shortest wavelength UV filter for the OM telescope). Clearly good correlations are found for all three intra-bands cases.

Similarly, Optical/UV and X-ray flux variabilities are checked by plotting soft X-ray vs V, and soft X-ray vs UVW1 which are shown in the left and middle panels of the bottom row of Fig. 4. These plots do not show any correlations, but there is good correlation between the V and UVW1 counts. From this analysis, we conclude that the variability within the X-ray, optical & UV bands are closed related to each other and further that the optical emission follows the same trend as UV emission. But there is no obvious correlation between the variability trends for the X-ray and the Optical/UV emissions. We also calculated correlation coefficients; they and their corresponding null hypothesis tests for each pair of combinations are given in Table 3.

Table 3. Variability Correlations between Optical, UV and X-ray bands

Bands	Correlation coefficient	Null hypothesis
Soft−Hard X-ray	0.9207	0.0
B-V	0.8845	0.0001
UVW1−UVW2	0.9862	0.00
Soft X-ray−V	-0.2308	0.4272
Soft X-ray−UVW1	-0.0012	0.9968
UVW1−V	0.9376	0.0

4.4 X-ray Hardness Ratio

The hardness ratio is evaluated by dividing hard band (4−10 keV) count rates by soft band (0.3−2 keV) count rates. To study the spectral evolution of the source, we examined patterns in the hardness ratio as a function of 0.3−10 keV count rates in the X-ray domain for different time spans. During this period of 12 years for which XMM−Newton observed 3C 273, the source has continuously evolved through spectral variations that are plotted in Fig. 5. These are best understood in terms of changes in the relative strength of particle acceleration and synchrotron cooling processes in X-ray emitting regions in 3C 273.

The results of this analysis provides a model independent spectral variability study of the source. Any loop occurring in the spectral hardness – flux representation, whether it is clockwise or anti-clockwise gives information about the leading emission mechanism during that period by considering the corresponding flux emitted at that time. So we plotted the hardness ratio points against the total X-ray count rates to see if any any loops appeared in the plot. Once a loop was visible in the plot, we terminated the plotting and marked that time span as an epoch and began a search for subsequent loops. In this process, we sometimes had to consider a single hardness ratio point as marking both the end of one loop plot and the beginning of another to best indicate the complete loops.

The widely accepted picture for the X-ray emission is that shock propagation in the relativistic jet is responsible for accelerating particles to extremely high energies, and when these highly relativistic particles encounter an inhomogeneous, twisted magnetic field in the jet, significant synchrotron emission occurs into the X-ray band, which dominates the cooling process. In Fig. 5, it is seen that in Epoch-1, the time span of June 2000 to December 2001, we observed an anti-clockwise loop (or hard-lag). This indicates that during that period particles were being accelerated to their highest speeds. We again have indications of the particles being accelerated in the internal shock outflow within the jet from epoch-2 (December 2002 to June 2003) and Epoch-3 (July 2003 to January 2007). Excluding Epoch−4 (January 2007 to December 2008), in Epoch−5, which spans over (6 December 2007−16 July 2012) too we found an anticlockwise loop in the spectral−flux representation indicating dominance of the particle acceleration mechanism. Only Epoch-4 shows a soft-lag and clockwise loop, which provides evidence of the synchrotron cooling mechanism being dominant during that particular period.

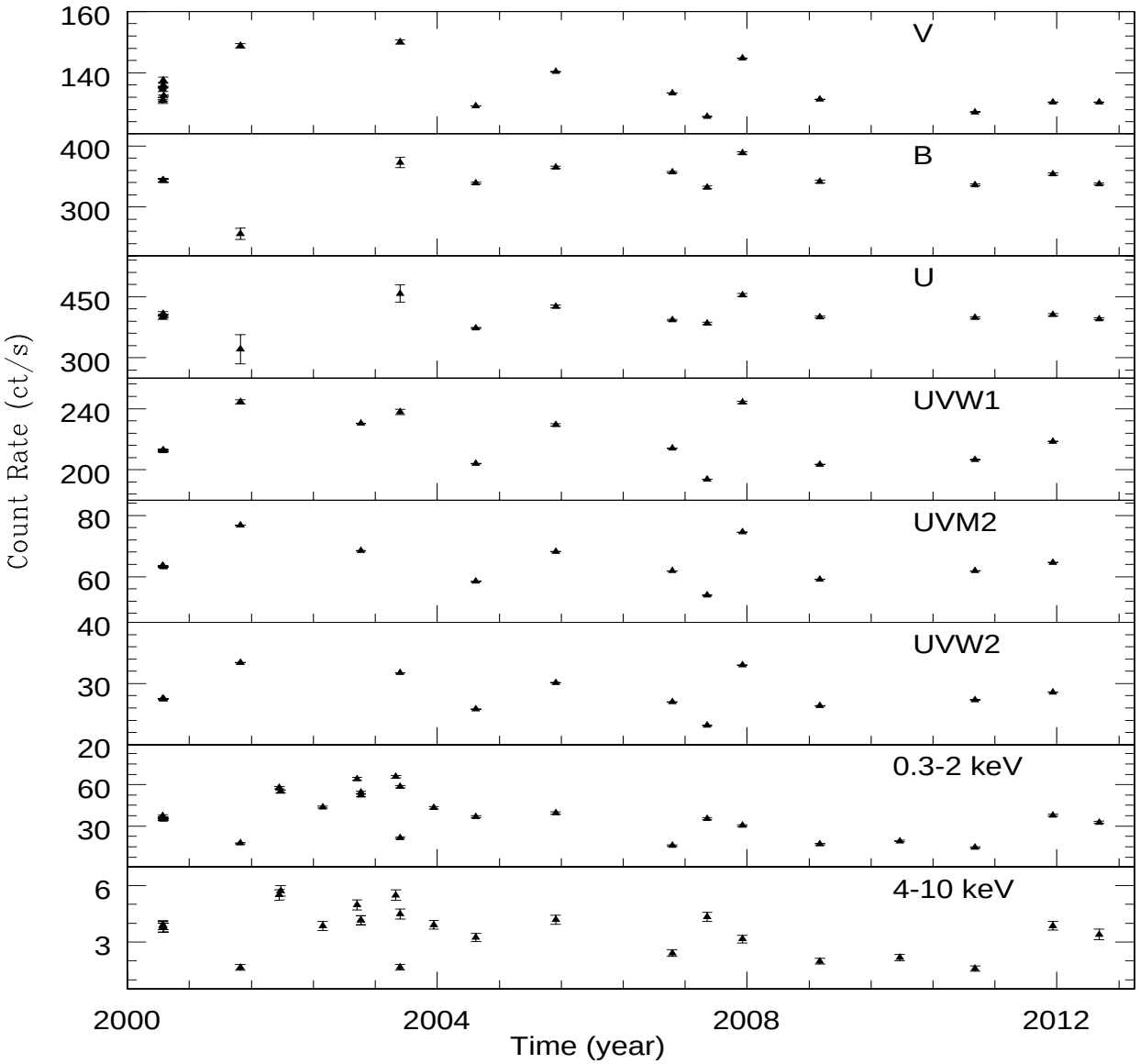

Figure 2. Optical/UV and X-ray long term variability (2000-2012). The lower panel shows two X-ray bands, hard and soft, respectively from the bottom. Three UV bands with increasing wavelength are plotted just above X-ray bands and in the upper panel, optical U, B and V bands are shown.

5 DISCUSSION AND CONCLUSIONS

In blazars, it is widely believed that variability is dominated by jet emission, which is significantly amplified by relativistic beaming. It has been believed most X-ray variability originates in a small region of the jet close to the SMBH of the blazar. The propagation of shock waves due to the fluctuations in hydromagnetically turbulent plasma in the relativistic jets can explain well the IDV and short term variability in blazars (e.g. Marscher 1996, 2014), though some intra-day variability may be also explained by instabilities due to magnetic fields or hot spotS on or above the accretion disk (e.g. Wiita 1996).

We have performed a time series analysis of the extensively studied blazar 3C 273 in X-ray and optical/UV bands for the data taken from XMM−Newton over a time period of more than a decade. For our analysis, we first plotted the $0.3 - 10$ keV light curves of the source, shown in Fig. 1. The blazar pointed observation period varied from 4.9ks for the shortest stare to 88.5ks for the longest. To study the IDV of the source in this period we have estimated the variability amplitude for all these observations and gave the results in Table 2. Only a few of these light curves showed even moderate flux variability, which only attained a maximum fractional rms variability of 2.6 per cent. Unsurprisingly, those observations, which were carried out for a longer period of times ($>$ 25 ks) gave more detectable variations, with $\mathrm{F}_{var} > 1$ per cent, while that lasted lees than 25 ks showed values of F_{var} below 1 per cent with errors large enough to make them indistinguishable from null variations.

Over longer times we saw that 3C 273 is highly variable in all bands that XMM−Newton measured in the X-ray, UV and optical.

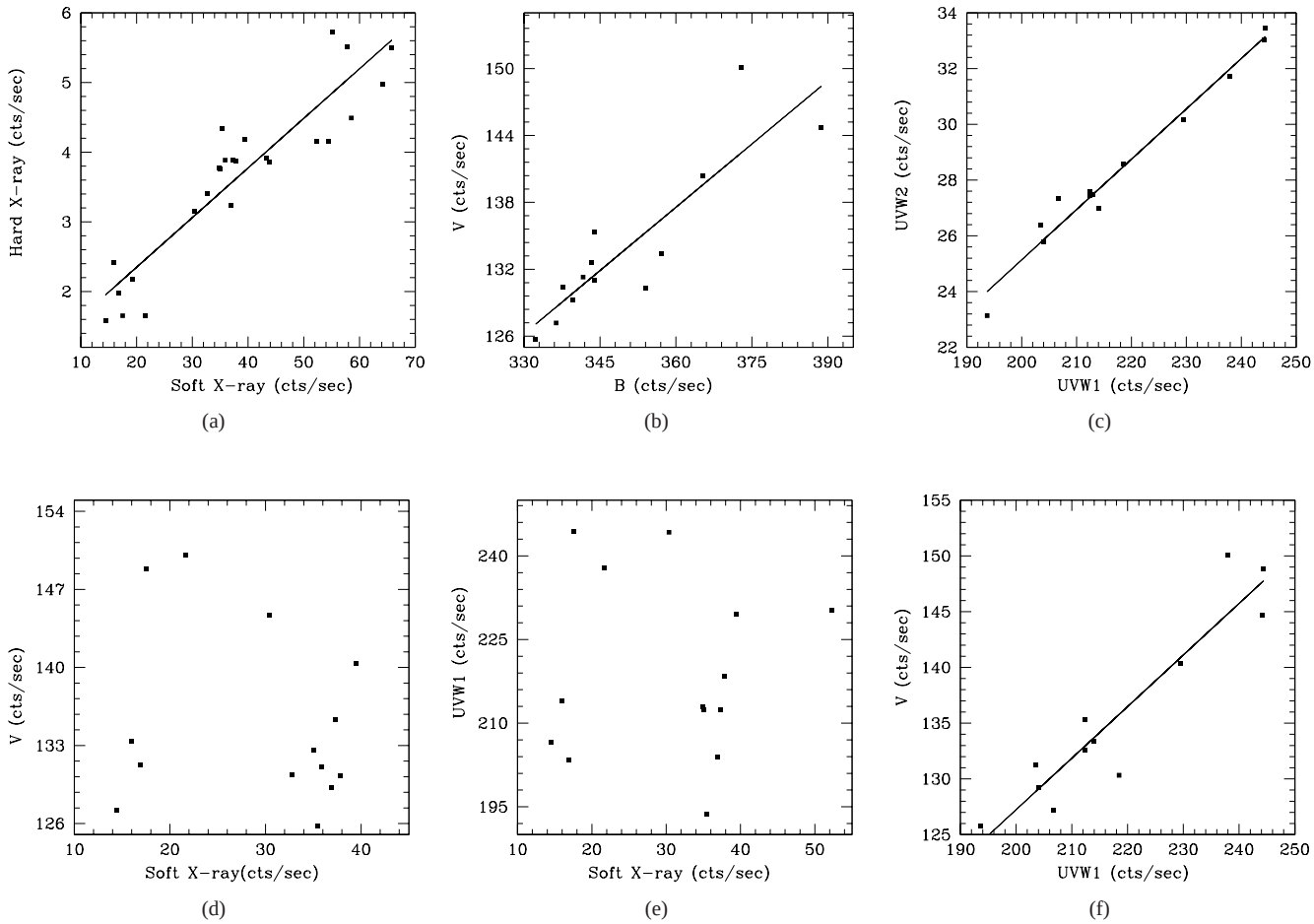

Figure 4. Correlations in variability between different optical, UV and X-ray bands.

In the Optical/UV bands, the variability amplitude decreases from UV to optical and was minimum for the V band, which is the lowest frequency measured. This can be understood simply in terms of the expectation that for synchrotron emission the more highly energetic particles cool more rapidly via the synchrotron and inverse Compton processes than do the less energetic ones. However, in the case of X-ray emission, variability in the soft band is higher than that in the hard band.

From our study of the variability relations between different bands, we see that soft and hard X-ray bands follow each other tightly, as shown in Fig. 4(a), indicating that their emission originates from same electron population. This doesn't answer the question as to whether the soft band follows the hard band of vice versa. The answer could in principle be found by computing the discrete correlation function (DCF) between these two bands as it would give the time difference as positive or negative lag between these emissions of corresponding bands. Unfortunately, we could not do a DCF analysis for this 3C 273 data, as they are quite poorly and irregularly sampled, so any computed DCF would be only too likely to indicate spurious correlations. The optical and UV bands too show correlation between their emissions, again indicating that these two bands are emitted from same region, but they are not correlated with X-ray band. Although for most blazars there is evidence that the X-ray emission is from the high energy tail of the synchrotron emission, which just extends the UV band to the X-ray (Jester et al. 2007), but apparently during the period, 2000–2012 this FSRQ apparently did not follow that scenario. In the local environment of 3C 273, there might be two electron populations with two different upper limits to their Lorentz factors such that the one with higher energetic particles is emitting in both the soft and hard X-ray bands while the other one with comparatively lower energetic particles is responsible for optical/UV emission.

Antilockwise loops in the hardness ratio vs 0.3−10 keV flux representation, which may also be referred to as the spectral index−flux representation, usually reveals a hard lag between the two emissions indicating that the soft band leads the hard band, yeilds that the source's hard flux increases more than soft flux with increasing total flux. This implies that during those periods particle acceleration mechanism was dominating over synchrotron mechanism for the emission observed in X-ray band.

To check the variation of flux over the observing time span we plotted the mean count rate of individual observations against modified Julian date. If one discounts some observations at the start and end of the totality of the measurements, the source shows a trend of flux decreasing (Fig. 3).

In this paper we have studied X-ray and optical/UV variability properties of the blazar 3C 273 with observations taken by the XMM−Newton satellite since its launch through the year 2012. We made use of all available data in the Public XMM−Newton data archive. We use the Epic/pn detector data for our X-ray study and the simultaneous OM data to study the source in different optical and UV bands for learn more about the physical processes produc-

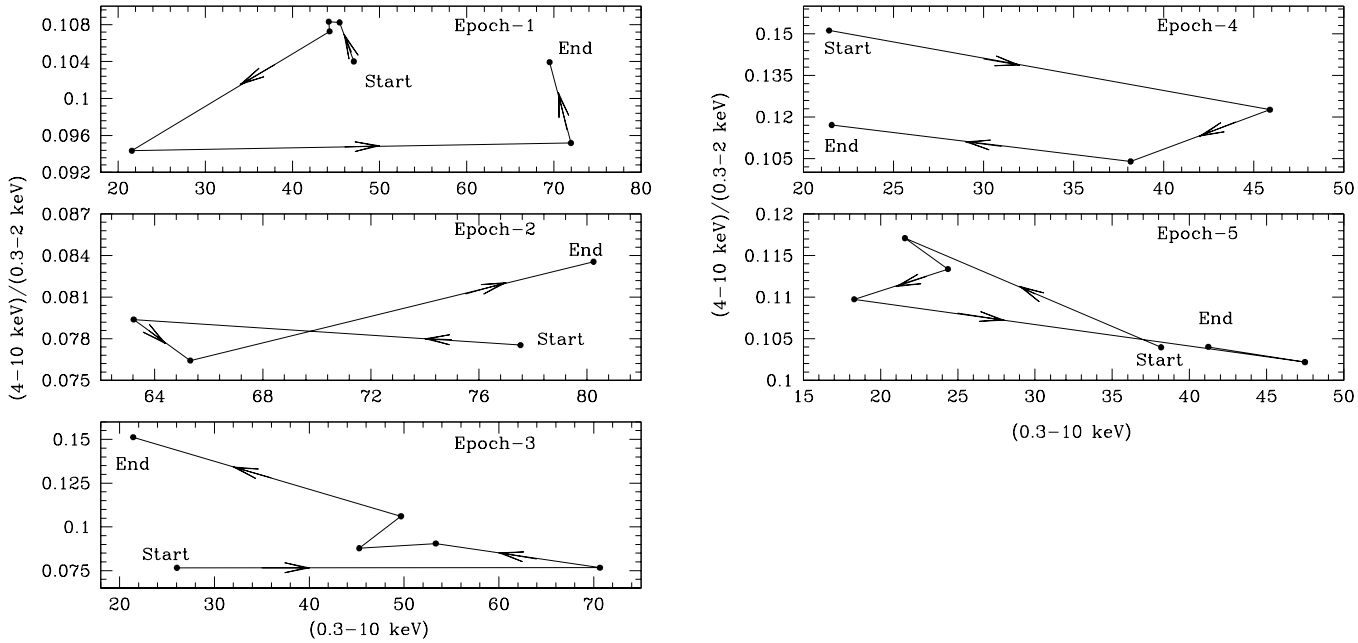

Figure 5. Spectral evolution of 3C 273 in different epochs. Arrows indicate the directions of the loops. Here the term epoch in the plots represent different time intervals during which the data were acquired for each corresponding loop: epoch−1 =13.06.2000−22.12.2001; epoch−2 =17.12.2002−18.06.2003; epoch−3 =07.07.2003−12.01.2007; epoch−4 =12.01.2007− 09.12.2008; epoch−5 = 06.12.2007−16.07.2012. The clockwise and anticlockwise loops are distinct and closed or nearly so, presenting a clear evidence of alternate acceleration and cooling mechanism.

ing the radiation. Our study of this fascinating source regarding its behaviour in different energy bands over this extended period shows high flux variation in long term in all the bands, but the Optical/UV flux variability is much higher than that in X-ray bands. Optical and UV variability depends on frequency, and increases with increasing frequency, as found in previous studies. But at the same time, the source follows the opposite frequency dependency of variability in the case X-ray emissions. During this observed 12 year interval the source shows evidence of both synchrotron cooling and particle acceleration mechanisms dominating the emission during different periods. No relation between X-ray and optical/UV emissions is found, supporting the scenario where two independent particle populations are present in its local emitting regions.

ACKNOWLEDGEMENTS

We thank the referee for detailed and thoughtful comments which helped us to improve the manuscript. We acknowledge the Department of Science & Technology (DST), India, for supporting this work with grants under the Women Scientist scheme-A (WOS–A). This research is based on observations taken with XMM–Newton, an ESA science mission with instruments and contributions directly funded by ESA Member Sates and NASA.

REFERENCES

Abdo A. A., et al., 2010, ApJ, 714, L73
Attridge J. M., Wardle J. F. C., Homan D. C., 2005, ApJ, 633, L85
Beaklini P. P. B., Abraham Z., 2014, MNRAS, 437, 489
Begelman M. C., Fabian A. C., Rees M. J., 2008, MNRAS, 384, L19
Brightman M., Nandra K., 2012, MNRAS, 422, 1166
Chernyakova M., et al., 2007, A&A, 465, 147
Collmar W., et al., 2000, A&A, 354, 513
Courvoisier T. J.-L., et al., 1987, A&A, 176, 197
Courvoisier T. J.-L., et al., 2003, A&A, 411, L343
Dai B. Z., et al., 2009, MNRAS, 392, 1181
Edelson R., Turner T. J., Pounds K., Vaughan S., Markowitz A., Marshall H., Dobbie P., Warwick R., 2002, ApJ, 568, 610
Edge D. O., Shakeshaft J. R., McAdam W. B., Baldwin J. E., Archer S., 1959, MmRAS, 68, 37
Espaillat C., Bregman J., Hughes P., Lloyd-Davies E., 2008, ApJ, 679, 182
Fan J. H., Peng Q. S., Tao J., Qian B. C., Shen Z. Q., 2009, AJ, 138, 1428
Fan J. H., Kurtanidze O., Liu Y., Richter G. M., Chanishvili R., Yuan Y. H., 2014, ApJS, 213, 26
Ghisellini G., Tavecchio F., 2008, MNRAS, 387, 1669
González-Martín O., Vaughan S., 2012, A&A, 544, A80
Gupta A. C., Banerjee D. P. K., Ashok N. M., Joshi U. C., 2004, A&A, 422, 505
Gupta A. C., Srivastava A. K., Wiita P. J., 2009, ApJ, 690, 216
Greve A., et al., 2002, A&A, 390, L19
Haardt F., et al., 1998, A&A, 340, 35
Jester S., Röser H.-J., Meisenheimer K., Perley R., 2005, A&A, 431, 477
Jester S., Meisenheimer K., Martel A. R., Perlman E. S., Sparks

W. B., 2007, MNRAS, 380, 828
Kaspi S., Smith P. S., Netzer H., Maoz D., Jannuzi B. T., Giveon U., 2000, ApJ, 533, 631
Kataoka J., Tanihata C., Kawai N., Takahara F., Takahashi T., Edwards P. G., Makino F., 2002, MNRAS, 336, 932
Kundu E., Gupta N., 2014, MNRAS, 444, L16
Leach C. M., McHardy I. M., Papadakis I. E., 1995, MNRAS, 272, 221
Liu L., Zhang Y., 2011, JApA, 32, 173
Mangalam A. V., Wiita P. J., 1993, ApJ, 406, 420
Mantovani F., Junor W., McHardy I. M., Valerio C., 2000, A&A, 354, 497
Marscher A. P., 1996, in Blazar Continuum Variability, eds. H. R. Miller, J. R. Webb, J. C. Noble, ASPC, 110, 248
Marscher A. P., 2014, ApJ, 780, 87
Mason K. O., et al., 2001, A&A, 365, L36
McHardy I. M., 2013, MNRAS, 430, L49
McHardy I., Lawson A., Newsam A., Marscher A., Robson I., Stevens J., 1999, MNRAS, 310, 571
McHardy I., Lawson A., Newsam A., Marscher A. P., Sokolov A. S., Urry C. M., Wehrle A. E., 2007, MNRAS, 375, 1521
Mohan P., Mangalam A., Chand H., Gupta A. C., 2011, JApA, 32, 117
Pacciani L., et al., 2009, A&A, 494, 49
Page K. L., Turner M. J. L., Done C., O'Brien P. T., Reeves J. N., Sembay S., Stuhlinger M., 2004, MNRAS, 349, 57
Paltani S., Türler M., 2005, A&A, 435, 811
Pietrini P., Torricelli-Ciamponi G., 2008, A&A, 479, 365
Rani B., Lott B., Krichbaum T. P., Fuhrmann L., Zensus J. A., 2013, A&A, 557, AA71
Sambruna R. M., Urry C. M., Tavecchio F., Maraschi L., Scarpa R., Chartas G., Muxlow T., 2001, ApJ, 549, L161
Savolainen T., Wiik K., Valtaoja E., Tornikoski M., 2006, A&A, 446, 71
Schmidt M., 1963, Natur, 197, 1040
Sikora M., 1994, ApJS, 90, 923
Soldi S., et al., 2008, A&A, 486, 411
Strüder L., et al., 2001, A&A, 365, L18
Swanenburg B. N., et al., 1978, Natur, 275, 298
Türler M., et al., 2006, A&A, 451, L1
Turner M. J. L., Courvoisier T., Staubert R., Molteni D., Trumper J., 1985, SSRv, 40, 623
Turriziani S., 2011, JPhCS, 280, 012005
Urry C. M., Padovani P., 1995, PASP, 107, 803
Vagnetti F., Turriziani S., Trevese D., 2011, A&A, 536, A84
Vaughan S., Edelson R., Warwick R. S., Uttley P., 2003, MNRAS, 345, 1271
Wagner S. J., Witzel A., 1995, ARA&A, 33, 163
Wen S.-l., Peng Z.-m., Fan J.-h., Xie G.-z., 2002, ChA&A, 26, 398
Wiita P. J., 1996, in Blazar Continuum Variability, eds. H. R. Miller, J. R. Webb, J. C. Noble, ASPC, 110, 42